Color-Coded Fluorescence Imaging of Lymph-Node Metastasis, Angiogenesis, and Its Drug-Induced Inhibition

Ryoichi Aki,[1,2,3] Yasuyuki Amoh,[2] Michael Bouvet,[2] Kensei Katsuoka,[2] and Robert M. Hoffman[1,3]*

[1]AntiCancer, Inc., 7917 Ostrow Street, San Diego, California 92111

[2]Department of Dermatology, Kitasato University School of Medicine, Kanagawa, Japan

[3]Department of Surgery, University of California, San Diego, 200 West Arbor Drive, San Diego, California 92103-8220

ABSTRACT

Lymph nodes are often the first target of metastatic cancer which can then remetastasize to distant organs. The progression of lymph node metastasis is dependent on sufficient blood supply provided by angiogenesis. In the present study, we have developed a color-coded imaging model to visualize angiogenesis of lymph nodes metastasis using green fluorescent protein (GFP) and red fluorescent protein (RFP). Transgenic mice carrying GFP under the control of the nestin promoter (ND-GFP mice) were used as hosts. Nascent blood vessels express GFP in these mice. B16F10-RFP melanoma cells were injected into the efferent lymph vessel of the inguinal lymph node of the ND-GFP nude mice, whereby the melanoma cells trafficked to the axillary lymph node. Three days after melanoma implantation, ND-GFP-expressing nascent blood vessels were imaged in the axillary lymph nodes. Seven days after implantation, ND-GFP-expressing nascent blood vessels formed a network in the lymph nodes. ND-GFP-positive blood vessels surrounded the tumor mass by 14 days after implantation. However, by 28 days after implantation, ND-GFP expression was diminished as the blood vessels matured. Treatment with doxorubicin significantly decreased the mean nascent blood vessel length per tumor volume. These results show that the dual-color ND-GFP blood vessels/RFP-tumor model is a powerful tool to visualize and quantitate angiogenesis of metastatic lymph nodes as well as for evaluation of its inhibition. J. Cell. Biochem. 115: 457–463, 2014.
© 2013 Wiley Periodicals, Inc.

KEY WORDS: lymph node metastasis; angiogenesis; melanoma; GFP; RFP; nestin; nude mice; transgenic; imaging

Lymph nodes are often the initial targets of metastatic cancer which can then remetastasize to more distant organs. The progression of lymph node metastasis depends on development of a sufficient blood supply. We have previously developed a color-coded tumor angiogenesis mouse model using nestin-driven green fluorescent protein (GFP) (ND-GFP) transgenic mice. In ND-GFP mice, nascent blood vessels are labeled with GFP [Amoh et al., 2004, 2005a, 2005b, 2006a, 2006b, 2006c, 2007, 2008; Hayashi et al., 2007a, 2007b, 2009; Hoffman, 2005, 2006; Hoffman and Yang, 2006; Ji et al., 2007]. The ND-GFP expressing structures are blood vessels, since they display the characteristic endothelial-cell-specific markers CD31 and von Willebrand factor. This model displays very early events in tumor angiogenesis and can be used for rapid anti-angiogenesis drug screening [Hoffman, 2006; Amoh et al., 2008].

In previous studies, we visualized tumor angiogenesis by dual-color fluorescence imaging in ND-GFP transgenic mice after transplantation of cancer cells expressing red fluorescent protein (RFP). ND-GFP was highly expressed in proliferating endothelial cells of nascent blood vessels in the growing tumor. ND-GFP expression was diminished in the vessels with increased blood flow. Progressive angiogenesis was readily visualized during tumor growth by GFP expression [Hoffman and Yang, 2006].

We observed that chemotherapy agents such as doxorubicin and gemcitabine inhibited the nascent tumor angiogenesis as well as tumor growth in the ND-GFP mice transplanted with RFP-expressing cancer cells. This model proved useful for simultaneous color-coded imaging of tumor growth and angiogenesis and evaluation of angiogenic inhibitors [Amoh et al., 2005a, 2005b, 2006a, 2006b, 2007, 2008; Hayashi et al., 2007a].

457

In the present study, a lymph node metastasis model of RFP melanoma was developed in the ND-GFP mice. Angiogenesis of the lymph node metastasis was imaged over time as well as its drug-induced inhibition.

MATERIALS AND METHODS

ND–GFP TRANSGENIC MICE

Transgenic mice carrying GFP under the control of the nestin promoter (ND-GFP mice) were originally obtained from Dr. G. Enikolopov (Cold Spring Harbor Laboratory, Cold Spring Harbor, NY) [Mignone et al., 2004] and bred at AntiCancer, Inc. Animals were kept in a barrier facility under HEPA filtration. Mice were fed an autoclaved laboratory rodent diet (Tecklad LM-485, Western Research Products). All animal studies were conducted in accordance with the principles and procedures outlined in the NIH Guide for the Care and Use of Animals under assurance A3873-01.

RFP VECTOR PRODUCTION

For RFP retrovirus production, the HindIII/NotI fragment from pDsRed2 (Clontech Laboratories, Inc.), containing the full-length RFP cDNA, was inserted into the HindIII/NotI site of pLNCX2 (Clontech Laboratories) that has the neomycin resistance gene to establish the pLNCX2-DsRed2 plasmid. PT67, an NIH3T3-derived packaging cell line (Clontech Laboratories) expressing the 10 Al viral envelope, was cultured in DMEM (Irvine Scientific) supplemented with 10% heat-inactivated fetal bovine serum (FBS; Gemini Bio-products). For vector production, PT67 cells, at 70% confluence, were incubated with a precipitated mixture of LipofectAMINE reagent (Life Technologies, Inc., Grand Island, NY) and saturating amounts of pLNCX2-DsRed2 plasmid for 18 h. Fresh medium was replenished at this time. The cells were examined by fluorescence microscopy 48 h after transduction. For selection of a clone producing high amounts of a RFP retroviral vector (PT67-DsRed2), the cells were cultured in the presence of 200 to 1,000 μg/mL G418 (Life Technologies), increased stepwise, for 7 days [Hoffman and Yang, 2006].

RFP GENE TRANSDUCTION OF TUMOR CELL LINES

For RFP gene transduction, 70% confluent B16F10 melanoma cells were used. In brief, cancer cells were incubated with a 1:1 precipitated mixture of retroviral supernatants of PT67-RFP cells and RPMI 1640 (Mediatech, Inc.) containing 10% FBS for 72 h. Fresh medium was replenished at this time. Cells were harvested with trypsin/EDTA 72 h after transduction and sub-cultured at a ratio of 1:15 in selective medium, which contained 200 μg/mL G418. The level of G418 was increased stepwise up to 800 μg/mL. RFP-expressing cancer cells were isolated with cloning cylinders (Bel-Art Products) using trypsin/EDTA and amplified by conventional culture methods [Hoffman and Yang, 2006].

MOUSE MODEL FOR IMAGING METASTATIC LYMPH NODE ANGIOGENESIS

ND-GFP transgenic mice 6 to 8 weeks old were used. The mice were anesthetized with a ketamine mixture (10 μL ketamine HCL, 7.6 μL xylazine, 2.4 μL acepromazine maleate, and 10 μL H_2O) via subcutaneous injection. The inguinal lymph node connects to the axillary lymph node via lymphatic vessels in the mouse (Fig. 1a,b). A rectangular skin flap was made in the inguinal region (Fig. 1c). The subcutaneous connective tissue was separated from the skin flap without injuring the lymphatic vessels. Mice were laid flat and the skin flap was spread and fixed on a flat stand. B16F10-RFP cells (5×10^5) in 20 μL PBS were injected into the efferent lymph vessel of the inguinal lymph node with a 31G Insulin Syringe (BD Biosciences, Bedford, MA).

A total of 10 mice were used in this study. Five mice were injected with 20 μL PBS into the efferent lymph vessel of the inguinal lymph node as vehicle controls. After the mice were anesthetized with a ketamine mixture, the axillary lymph nodes of the mice were observed at days 0, 3, 7, 14, and 28 after injection of cancer cells. The axillary lymph node was exposed from the inner side with a rectangular skin flap [Yang et al., 2002] (Fig. 1d). Images were acquired as described below with the Olympus OV100 Small Animal Imaging System (Olympus Corp., Tokyo, Japan). There was not significant variation between mice at any time point.

At day-14 after implantation of B16F10-RFP melanoma cells, the axillary lymph nodes were excised. The lymph node specimens were divided into two parts; one for fluorescence microscopy and the other for paraffin sections. At the end of experiment, the mice were euthanized.

HISTOLOGICAL EXAMINATION

For histological studies, lymph node samples were put into IHC Zinc Fixative (BD Biosciences, Bedford, MA) for 72 h at room temperature. All of the samples were subsequently processed through alcohol dehydration and paraffinization. Lymph node samples were embedded in paraffin and sectioned at 4 μm. The slides were stained by H&E, and examined microscopically.

IMMUNOHISTOCHEMICAL STAINING

Localization of CD31 in the nascent blood vessels of the metastatic lymph nodes was detected with the anti-rat immunoglobulin horseradish peroxidase detection kit (BD Biosciences, San Diego, CA) following the manufacturer's instructions. Anti-CD31 monoclonal antibody (550274) was purchased from BD Biosciences (San Diego, CA).

FLUORESCENCE MICROSCOPY

Fluorescence microscopy was carried out with an IX71 inverted microscope (Olympus Corp., Tokyo, Japan) equipped with a mercury lamp power supply. The microscope had a GFP filter set.

MEASUREMENT OF LENGTH OF NESTIN–POSITIVE NASCENT BLOOD VESSELS AND EVALUATION OF ANTI–ANGIOGENIC EFFICACY OF DOXORUBICIN

ND-GFP transgenic mice, 6 to 8 weeks old, were used. B16F10-RFP cells (5×10^5) in 20 μL PBS were injected as described above. The mice were given daily i.p. injections of doxorubicin (5 μg/g) or 0.9% NaCl solution (vehicle controls) at days 0, 1, and 2 after implantation of cancer cells. This protocol was used in order to minimize doxorubicin toxicity. A total of 10 mice were used in this study. Five mice were injected with doxorubicin, and the other mice were injected with 0.9% NaCl solution as vehicle controls. The mice were
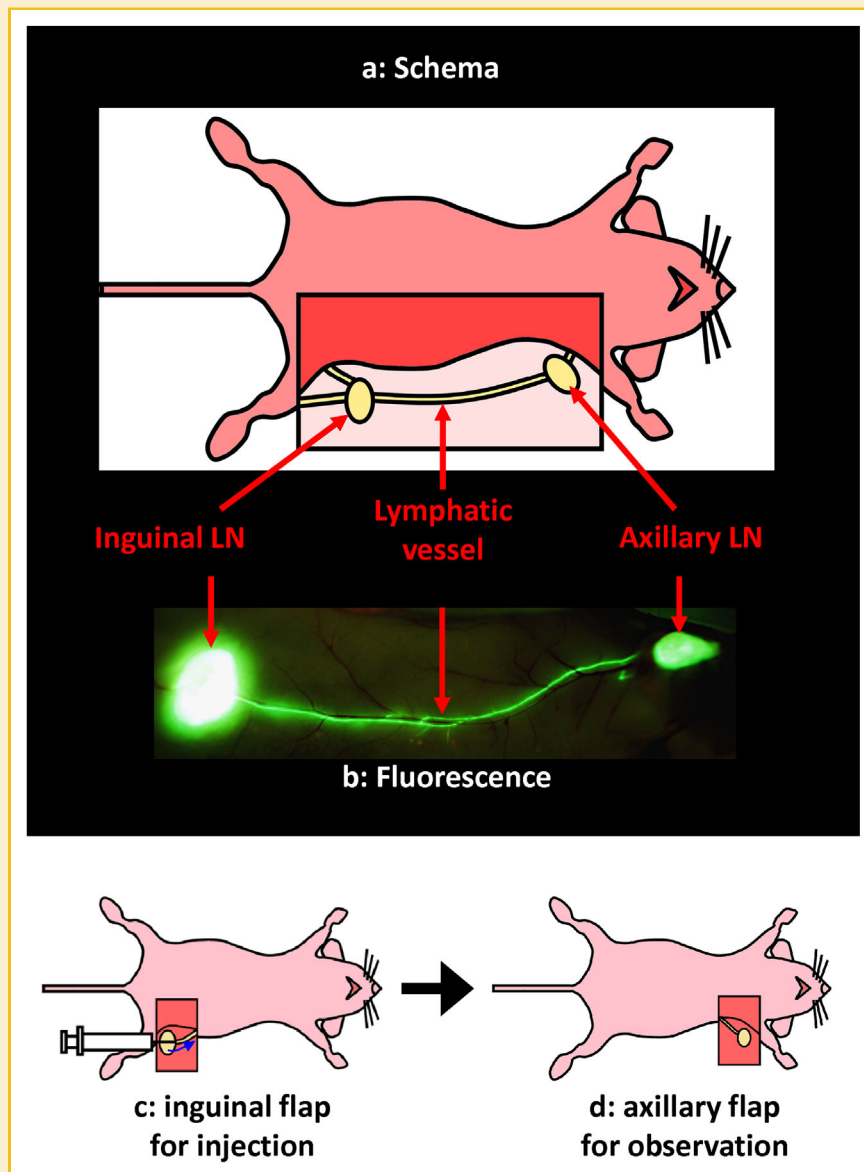
Fig. 1. Inguinal–axillary lymphatic system of the mouse. (a) Schema of the inguinal lymph node connecting to the axillary lymph node via lymphatic vessels. (b) A fluorescence view after injection of FITC to show the anatomy of this lymphatic system. One mg/mL FITC was injected into the efferent lymph vessel of the inguinal lymph node. c: A small rectangular skin flap was made in the the inguinal region when cancer cells were injected into the efferent lymph vessel of the inguinal lymph node. d: A small rectangular skin flap was made in the axillary region when the axillary lymph node was observed. Small skin flaps were necessary to minimize the effects of surgery on the lymphatic system.

anesthetized with a ketamine mixture, and the axillary lymph nodes were excised at day 8 after implantation of the B16F10-RFP melanoma cells. At the end of the experiment, the mice were euthanized. The lymph nodes were measured in three dimensions with calipers, and the lymph node volume (mm^3) was calculated with the formula $V = 0.52 \times \text{length} \times \text{width} \times \text{height}$ with an ellipsoid approximation. The lymph node was flattened between the slide and coverslip. Angiogenesis was quantified in the lymph node by measuring the length of ND-GFP nascent blood vessels in all fields under fluorescence microscopy. All fields at 40× or 100× magnification were measured in order to calculate the total length of ND-GFP-positive nascent blood vessels. The vessel density was calculated by the total length of ND-GFP nascent blood vessels divided by the tumor volume (mm^3).

STATISTICAL ANALYSIS

The experimental data are expressed as the mean ± SD. Statistical analysis was performed using the two-tailed Student's *t*-test.

RESULTS AND DISCUSSION

EARLY LYMPH NODE TUMOR ANGIOGENESIS

Immediately after injection into the inguinal lymph node, B16F10-RFP melanoma cells trafficked to the axillary lymph node via afferent
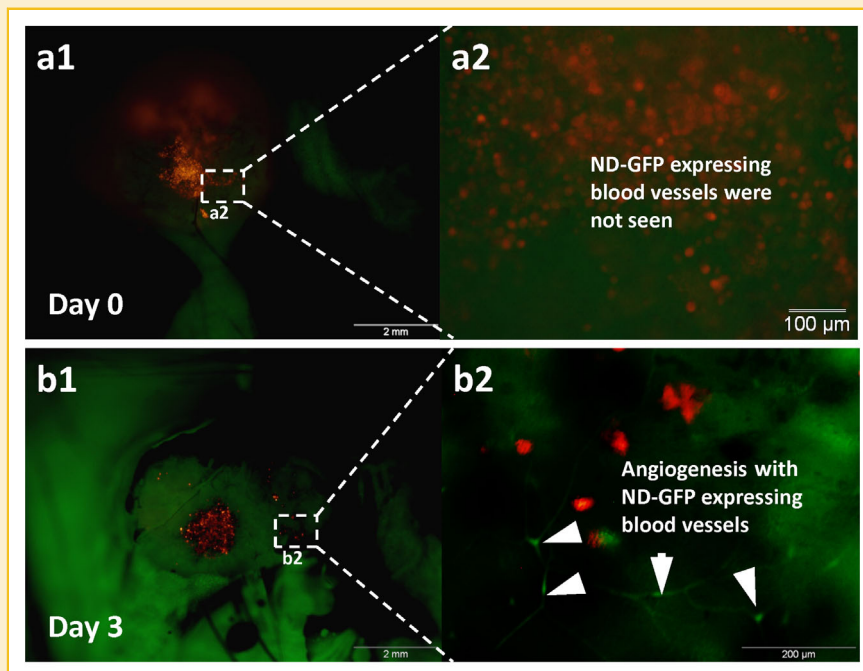
Fig. 2. Early tumor angiogenesis of lymph nodes visualized by color-coded imaging. a1, a2: Just after B16F10-RFP melanoma cell injection into the inguinal lymph node of ND-GFP transgenic mice, the axillary lymph node was directly imaged. a1: RFP-melanoma cells trafficked to the whole lymph node via afferent lymph vessels. Scale bars, 2 mm. a2: is the higher magnification of area of (a1) indicated by the white dashed box. ND-GFP-expressing blood vessels were not imaged. Scale bars, 200 μm. b1, b2: On day-3 after B16F10-RFP melanoma cell injection into the inguinal lymph node of ND-GFP transgenic mice, the axillary lymph node was directly observed. b1: Most of the RFP-melanoma cells disappeared, but some remained. Scale bars, 2 mm. (b2) is the higher magnification of area of (b1) indicated by the white dashed box. Angiogenesis with ND-GFP expressing blood vessels (white arrows) was observed. Scale bars, 200 μm.

lymph vessels (Fig. 2a1). At this time, ND-GFP expressing blood vessels were not yet present in the axillary lymph node (Fig. 2a2). At day-3 after injection, most of the RFP-melanoma cells had disappeared. However, some melanoma cells were observed to remain in the axillary lymph node (Fig. 2b1). At this time, ND-GFP-expressing blood vessels could be observed in the axillary lymph node (Fig. 2b2).

It is possible that some of the melanoma cells were rapidly cleared from the metastatic lymph nodes and some of the cells may not have survived, as we have previously observed with other cancer cell types [Tsuji et al., 2006; Yamauchi et al., 2008; Kimura et al., 2010].

LATE-STAGE LYMPH NODE TUMOR ANGIOGENESIS

By day-7 after injection of cancer cells, ND-GFP-expressing blood vessels formed a network in the lymph node and were connected to the tumor mass (Fig. 3a). ND-GFP-expressing blood vessels were not observed in mice injected with PBS instead of cells (Fig. 3b). By day-14, ND-GFP-positive blood vessels surrounded the RFP-expressing tumor (Fig. 3c). In the PBS control group at day-14, ND-GFP-expressing blood vessels were not observed (Fig. 3d). Angiogenesis induced by the cancer cells in turn probably promoted rapid metastatic growth in the lymph node [Folkman, 1972]. By day-28 after injection of cancer cells, ND-GFP expression was diminished in the lymph node (data not shown). Figures 2 and 3 are representative mice analyzed at the indicated time points. There was not significant variation between mice at any time point.

HISTOLOGICAL, FLUORESCENCE, AND IMMUNOHISTOCHEMICAL ANALYSIS OF LYMPH ANGIOGENESIS

H&E staining showed duct structures in the tumor (Fig. 3e). The innermost layer of the duct was lined with endothelial cells. A frozen section showed the ND-GFP-expressing blood vessels under fluorescence microscopy (Fig. 3f). Nestin (Fig. 3f) and CD31 (Fig. 3g) were colocalized in the blood vessels. These results showed ND-GFP-expressing blood vessels are CD31 positive.

EFFICACY OF DOXORUBICIN ON LYMPH NODE TUMOR ANGIOGENESIS

At day-8 after cancer-cell implantation, the lymph node metastasis had ND-GFP-expressing blood vessels. Treatment with doxorubicin decreased the RFP-expressing tumor volume in the lymph nodes (Fig. 4a1,b1). In addition, the number of ND-GFP-expressing blood vessels was much less in the doxorubicin-treated animals (Fig. 4b2) than in NaCl-injected control mice (Fig. 4a2). Thus, treatment with doxorubicin significantly decreased nascent blood vessel formation, measured by mean nascent blood vessel length per tumor volume (Fig. 4c; $^*P < 0.05$ versus NaCl solution-injected mice).

von Andrian et al. [2006] showed the structure of blood vessels in lymph nodes using angiography. McElroy et al. [2009] combined the staining specificity of the LYVE-1 monoclonal antibody which binds to murine lymphatic endothelial cells, with in vivo fluorescence imaging to enable real-time color-coded imaging of lymphatic vessels and cancer-cell trafficking in the vessels.
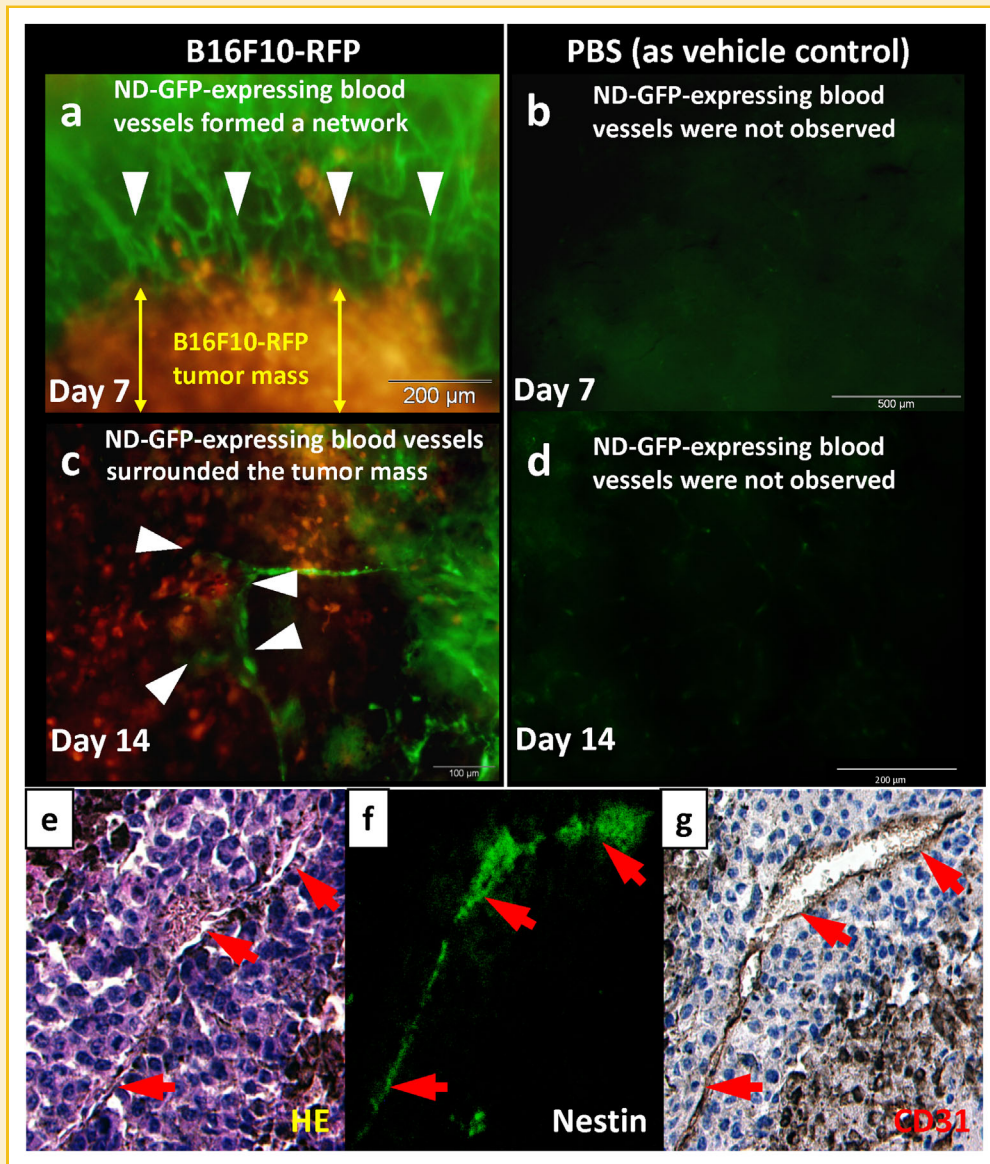
Fig. 3. Late–stage tumor angiogenesis of lymph nodes visualized by color–coded imaging. a: On day–7 after B16F10–RFP melanoma injection into the inguinal lymph node of ND–GFP transgenic mice, the axillary lymph nodes were directly imaged. ND–GFP–expressing blood vessels (white arrows) formed a network in the lymph node and connected to the tumor mass (yellow arrows). b: On day–7 after PBS injection, without melanoma cells, into the inguinal lymph node of ND–GFP transgenic mice, the axillary lymph node was directly imaged. ND–GFP–expressing blood vessels were not observed. c: On day–14 after B16F10–RFP melanoma–injection into the inguinal lymph node of ND–GFP transgenic mice, the axillary lymph node was directly imaged. ND–GFP–expressing blood vessels (white arrows) surrounded the tumor. d: On day–14 after PBS injection into the inguinal lymph node of ND–GFP transgenic mice, the axillary lymph node was directly imaged. In this control group, ND–GFP–expressing blood vessels were not observed by day–14. Scale bars, 200 μm (a–d). e–g: Representative microscopic images for H&E staining (e), fluorescence (f), and immunohistochemical staining (g). e: Some duct structures were observed in the tumor (red arrow). The innermost layer of the duct was lined with endothelial cells. f: A frozen section showed the ND–GFP blood vessels (red arrow). g: CD31 immunohistochemical stain (red arrow). Nestin (f; red arrow) and CD31 (g; red arrow) were colocalized in the blood vessels in stained sister sections. These results showed ND–GFP–expressing blood vessels are CD31 positive. Scale bars, 100 μm (a–h).

The present study shows that B16F10-RFP melanoma cells induced ND-GFP-expressing blood vessels in the axillary lymph node which could be observed by day-3 after melanoma cell implantation (Fig. 2b1,b2). Seven days after implantation, ND-GFP-expressing blood vessels formed a network (Fig. 3a). ND-GFP-expressing blood vessels surrounded the tumor mass 14 days after tumor implantation (Fig. 3c). However, by 28 days after implantation, ND-GFP-expression in blood vessels was completely extinguished because the blood vessels had matured (data not shown).

The ND-GFP-expressing structures were blood vessels, since they displayed the characteristic endothelial-cell-specific markers CD31 and von Willebrand factor [Amoh et al., 2004]. We previously demonstrated that nestin is a marker for proliferating endothelial cells in nascent blood vessels [Amoh et al., 2004, 2005a]. In the present
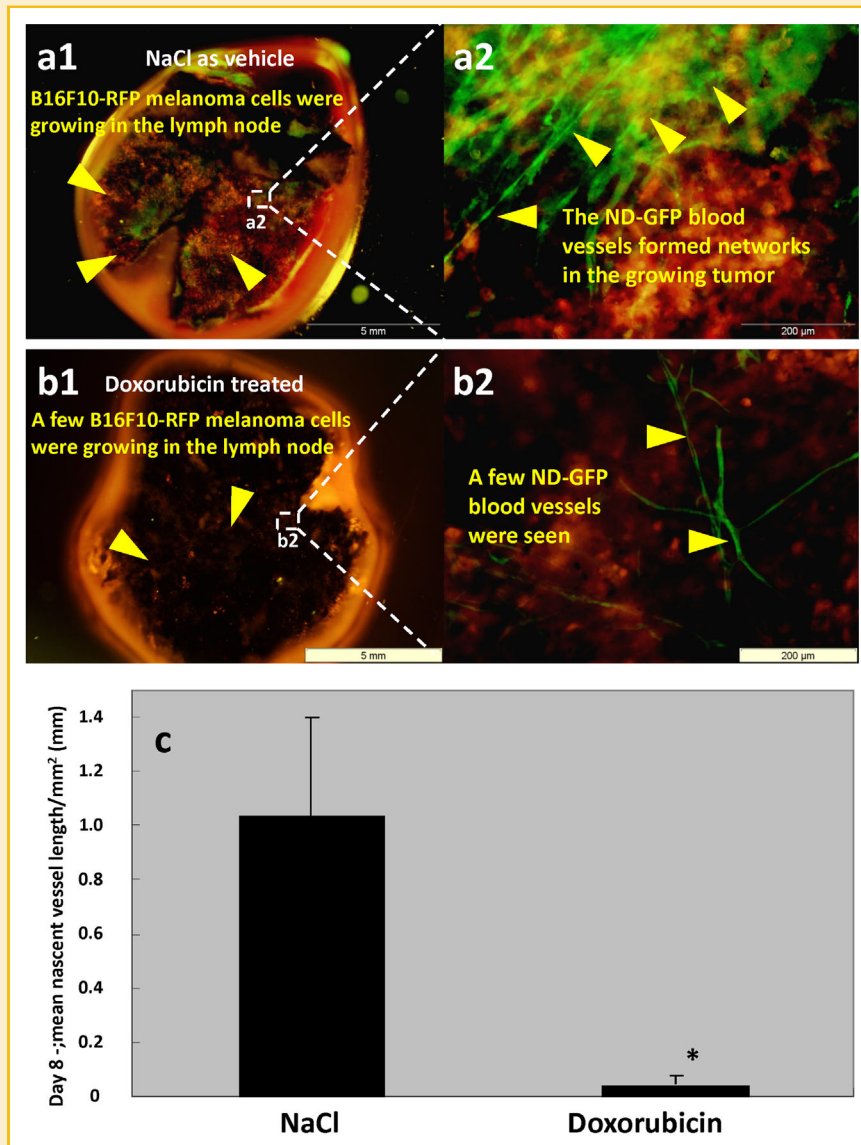
Fig. 4. Evaluation of anti-angiogenic efficacy of doxorubicin. a,b: On day-8 after B16F10–RFP cell implantation into the inguinal lymph node of ND–GFP transgenic mice, fresh biopsied tissue of the lymph node was observed by fluorescence imaging. a1: The mice were given daily i.p. injections of NaCl as vehicle control at days 0, 1, and 2 after injection of melanoma cells. B16F10–RFP melanoma cells (yellow arrows) were growing in the lymph node. Scale bars, 5 mm. (a2) is the higher magnification of area of (a1) indicated by the white dashed box. ND–GFP blood vessels (yellow arrows) formed networks in the growing tumor. Scale bars, 200 μm. b1: The mice were given daily i.p. injections of 5 μg/g of doxorubicin at days 0, 1, and 2 after injection of cancer cells. A few B16F10–RFP melanoma cells (yellow arrows) were growing in the lymph node. Scale bars, 5 mm. (b2) is the higher magnification of area of (b1) indicated by the white dashed box. A few ND–GFP blood vessels (yellow arrows) can be seen. The number of ND–GFP-expressing blood vessels was much less in the doxorubicin–treated animals (b2) than in NaCl–injected control mice (a2). Treatment with doxorubicin decreased nascent blood vessel formation as well as tumor volume. Scale bars, 200 μm. c: By day-8 after implantation of melanoma cells, treatment with doxorubicin significantly decreased the mean nascent blood vessel length per tumor volume ($P < 0.05$).

study, we showed that nestin and CD31 expression co-localized (Fig. 3e–g). This fact suggests that ND-GFP-expressing structures are angiogenic blood vessels. Thus, nestin is a useful marker for angiogenesis of lymph node metastasis. Blood vessels in GFP-labeled tumors can also be visualized by dark contrast, including by non-invasive imaging [Yang et al., 2001].

The color-coded model of lymph angiogenesis was used to evaluate angiogenic inhibitors. Treatment with doxorubicin significantly decreased the mean nascent blood vessel length per tumor volume (Fig. 4c).

These results show the dual-color ND-GFP-mouse/RFP-tumor model is a powerful tool to visualize and quantitate angiogenesis of metastatic lymph nodes and to evaluate angiogenesis inhibitors.

A model of inter-lymph-node metastasis has recently been developed using a mouse strain with remarkable lymphadenopathy such that the size of the mouse lymph nodes approximates those of

humans. The strong advantage of this model is the ease of imaging of the large metastatic lymph nodes [Li et al., 2013]. The strong advantage of our model is that by using cancer cells labeled with one color fluorescent protein and blood vessels labeled with a fluorescent protein of another color [Yang et al., 2003, 2004, 2007, 2009], simultaneous color-coded imaging of metastatic tumor growth and angiogenesis is made possible at cellular resolution. An exciting future possibility is to cross the lymphadenopathy mouse with the ND-GFP mouse to produce an ND-GFP lymphadenopathy mouse for color-coded real-time imaging of lymph-node metastasis and angiogenesis.

ACKNOWLEDGMENTS

REFERENCES

Amoh Y, Li L, Yang M, Moossa AR, Katsuoka K, Penman S, Hoffman RM. 2004. Nascent blood vessels in the skin arise from nestin-expressing hair follicle cells. Proc Natl Acad Sci USA 101:13291–13295.

Amoh Y, Li L, Yang M, Jiang P, Moossa AR, Katsuoka K, Hoffman RM. 2005a. Hair follicle-derived blood vessels vascularize tumors in skin and are inhibited by doxorubicin. Cancer Res 65:2337–2343.

Amoh Y, Yang M, Li L, Reynoso J, Bouvet M, Moossa AR, Katsuoka K, Hoffman RM. 2005b. Nestin-linked green fluorescent protein transgenic nude mouse for imaging human tumor angiogenesis. Cancer Res 65:5352–5357.

Amoh Y, Li L, Tsuji K, Moossa AR, Katsuoka K, Hoffman RM, Bouvet M. 2006a. Dual-color imaging of nascent blood vessels vascularizing pancreatic cancer in an orthotopic model demonstrates antiangiogenesis efficacy of gemcitabine. J Surg Res 132:164–169.

Amoh Y, Nagakura C, Maitra A, Moossa AR, Katsuoka K, Hoffman RM, Bouvet M. 2006b. Dual-color imaging of nascent angiogenesis and its inhibition in liver metastases of pancreatic cancer. Anticancer Res 26:3237–3242.

Amoh Y, Bouvet M, Li L, Tsuji K, Moossa AR, Katsuoka K, Hoffman RM. 2006c. Visualization of nascent tumor angiogenesis in lung and liver metastasis by differential dual-color fluorescence imaging in nestin-linked-GFP mice. Clin Exp Metastasis 23:315–322.

Amoh Y, Li L, Katsuoka K, Bouvet M, Hoffman RM. 2007. GFP-expressing vascularization of Gelfoam® as a rapid in vivo assay of angiogenesis stimulators and inhibitors. Biotechniques 42:294–298.

Amoh Y, Katsuoka K, Hoffman RM. 2008. Color-coded fluorescent protein imaging of angiogenesis: The AngioMouse models. Curr Pharm Des 14:3810–3819.

Folkman J. 1972. Anti-angiogenesis: New concept for therapy of solid tumors. Ann Surg 175:409–416.

Hayashi K, Yamauchi K, Yamamoto N, Tsuchiya H, Tomita K, Amoh Y, Hoffman RM, Bouvet M. 2007a. Dual-color imaging of angiogenesis and its inhibition in bone and soft tissue sarcoma. J Surg Res 140:165–170.

Hayashi K, Jiang P, Yamauchi K, Yamamoto N, Tsuchiya H, Tomita K, Moossa AR, Bouvet M, Hoffman RM. 2007b. Real-time imaging of tumor-cell shedding and trafficking in lymphatic channels. Cancer Res 67:8223–8228.

Hayashi K, Yamauchi K, Yamamoto N, Tsuchiya H, Tomita K, Bouvet M, Wessels J, Hoffman RM. 2009. A color-coded orthotopic nude-mouse treatment model of brain-metastatic paralyzing spinal cord cancer that induces angiogenesis and neurogenesis. Cell Prol 42:75–82.

Hoffman RM. 2005. The multiple uses of fluorescent proteins to visualize cancer in vivo. Nat Rev Cancer 5:796–806.

Hoffman RM. 2006. AngioMouse: Imageable models of angiogenesis. In: Staton CA, Lewis C, Bicknell R, editors. Angiogenesis assays: A critical appraisal of current techniques. Hoboken, NJ: Wiley and Sons. pp 293–310.

Hoffman RM, Yang M. 2006. Color-coded fluorescence imaging of tumor-host interactions. Nat Protoc 1:928–935.

Ji Y, Hayashi K, Amoh Y, Tsuji K, Yamauchi K, Yamamoto N, Tsuchiya H, Tomita K, Bouvet M, Hoffman RM. 2007. The camptothecin derivative CPT-11 inhibits angiogenesis in a dual-color imageable orthotopic metastatic nude mouse model of human colon cancer. Anticancer Res 27:713–718.

Kimura H, Hayashi K, Yamauchi K, Yamamoto N, Tsuchiya H, Tomita K, Kishimoto H, Bouvet M, Hoffman RM. 2010. Real-time imaging of single cancer-cell dynamics of lung metastasis. J Cell Biochem 109:58–64.

Li L, Mori S, Sakamoto M, Takahashi S, Kodama T. 2013. Mouse model of lymph node metastasis via afferent lymphatic vessels for development of imaging modalities. PLoS ONE 8:e55797.

McElroy M, Hayashi K, Garmy-Susini B, Kaushal S, Varner JA, Moossa AR, Hoffman RM, Bouvet M. 2009. Fluorescent LYVE-1 antibody to image dynamically lymphatic trafficking of cancer cells in vivo. J Surg Res 151:68–73.

Mignone JL, Kukekov V, Chiang AS, Steindler D, Enikolopov G. 2004. Neural stem and progenitor cells in *nestin-GFP* transgenic mice. J Comp Neurol 469:311–324.

Tsuji K, Yamauchi K, Yang M, Jiang P, Bouvet M, Endo H, Kanai Y, Yamashita K, Moossa AR, Hoffman RM. 2006. Dual-color imaging of nuclear-cytoplasmic dynamics, viability, and proliferation of cancer cells in the portal vein area. Cancer Res 66:303–306.

Von Andrian UH. 1996. Intravital microscopy of the peripheral lymph node microcirculation in mice. Microcirculation 3:287–300.

Yamauchi K, Yang M, Hayashi K, Jiang P, Yamamoto N, Tsuchiya H, Tomita K, Moossa AR, Bouvet M, Hoffman RM. 2008. Induction of cancer metastasis by cyclophosphamide pretreatment of host mice: An opposite effect of chemotherapy. Cancer Res 68:516–520.

Yang M, Baranov E, Li X-M, Wang J-W, Jiang P, Li L, Moossa AR, Penman S, Hoffman RM. 2001. Whole-body and intravital optical imaging of angiogenesis in orthotopically implanted tumors. Proc Natl Acad Sci USA 98:2616–2621.

Yang M, Baranov E, Wang J-W, Jiang P, Wang X, Sun F-X, Bouvet M, Moossa AR, Penman S, Hoffman RM. 2002. Direct external imaging of nascent cancer, tumor progression, angiogenesis, and metastasis on internal organs in the fluorescent orthotopic model. Proc Natl Acad Sci USA 99:3824–3829.

Yang M, Li L, Jiang P, Moossa AR, Penman S, Hoffman RM. 2003. Dual-color fluorescence imaging distinguishes tumor cells from induced host angiogenic vessels and stromal cells. Proc Natl Acad Sci USA 100:14259–14262.

Yang M, Reynoso J, Jiang P, Li L, Moossa AR, Hoffman RM. 2004. Transgenic nude mouse with ubiquitous green fluorescent protein expression as a host for human tumors. Cancer Res 64:8651–8656.

Yang M, Jiang P, Hoffman RM. 2007. Whole-body subcellular multicolor imaging of tumor-host interaction and drug response in real time. Cancer Res 67:5195–5200.

Yang M, Reynoso J, Bouvet M, Hoffman RM. 2009. A transgenic red fluorescent protein-expressing nude mouse for color-coded imaging of the tumor microenvironment. J Cell Biochem 106:279–284.